Evaluation of the effect of computed tomography scan protocols and freeform fabrication methods on bone biomodel accuracy

Kathryn L. Fitzwater, DVM; Denis J. Marcellin-Little, DEDV; Ola L. A. Harrysson, PhD; Jason A. Osborne, PhD; E. Christine Poindexter, BS

Objective—To assess the effect of computed tomography (CT) scan protocols (radiation amounts) and fabrication methods on biomodel accuracy and variability.

Sample—Cadaveric femur of a Basset Hound.

Procedures—Retroreconstructions (n = 158) were performed of 16 original scans and were visually inspected to select 17 scans to be used for biomodel fabrication. Biomodels of the 17 scans were made in triplicate by use of 3 freeform fabrication processes (stereolithography, fused deposition modeling, and 3-D printing) for 153 models. The biomodels and original bone were measured by use of a coordinate measurement machine.

Results—Differences among fabrication methods accounted for 2% to 29% of the total observed variation in inaccuracy and differences among method-specific radiation configurations accounted for 4% to 44%. Biomodels underestimated bone length and width and femoral head diameter and overestimated cortical thickness. There was no evidence of a linear association between thresholding adjustments and biomodel accuracy. Higher measured radiation dose led to a decrease in absolute relative error for biomodel diameter and for 4 of 8 cortical thickness measurements.

Conclusions and Clinical Relevance—The outside dimensions of biomodels have a clinically acceptable accuracy. The cortical thickness of biomodels may overestimate cortical thickness. Variability among biomodels was caused by model fabrication reproducibility and, to a lesser extent, by the radiation settings of the CT scan and differences among fabrication methods. (*Am J Vet Res* 2011;72:1178–1185)

The digital acquisition of detailed 3-D anatomic images is possible by use of CT scanning and computer-aided image-editing software. Realistic and anatomically accurate 3-D renderings can be constructed from cross-sectional CT data.[1,2] These renderings may be sized, oriented, and exported to manufacture replicas that may be used to facilitate the assessment of complex orthopedic, vertebral, and maxillofacial fractures and deformities; to plan deformity corrections; and to design and build custom orthopedic implants used to manage trauma and for limb sparing.[2–19] Also, 3-D computer models derived from CT or magnetic resonance imaging scans may be used as the basis of computer simulations of flow in cardiovascular and respiratory systems, finite element analyses of tissues in contact with implants, and design of custom scaffolds for tissue engineering of soft and hard tissues.[20–34] Computed tomography variables, including the intensity of radiation, helical versus transverse scanning protocols, slice thickness, pitch, and reconstruction algorithms most likely influence the accuracy of cross-sectional CT data.[35] Although model manufacturing historically was done by use of conventional milling methods, it is now often done with higher accuracy by use of FFF methods, including SLA, FDM, or 3DP.[36–38] Freeform fabri-

Abbreviations

3DP	3-D printing
CT	Computed tomography
FDM	Fused deposition modeling
FFF	Freeform fabrication
HU	Hounsfield units
SLA	Stereolithography

Received February 22, 2010.
Accepted July 2, 2010.
From the Department of Clinical Sciences (Fitzwater, Marcellin-Little) and the Veterinary Teaching Hospital (Poindexter), College of Veterinary Medicine, the Edward P. Fitts Department of Industrial and Systems Engineering (Harrysson), College of Engineering, and the Department of Statistics (Osborne), College of Agriculture and Life Sciences, North Carolina State University, Raleigh, NC 27606. Dr. Fitzwater's present address is Circle City Veterinary Specialty and Emergency Hospital, 9650 Mayflower Park Dr, Carmel, IN 46032-7957.
Supported by the College of Veterinary Medicine Clinical Initiative Grant, North Carolina State University, and by the Biomodeling Laboratory, Fitts Department of Industrial and Systems Engineering, North Carolina State University.
The authors thank Christina Crimi, Christopher Crimi, Erica Lee, Brad J. LaBarbera, Wesley E. Cox, Richard A. Daniels, Kassi K. Rose, Guha Prasanna Manogharan, Tim Vojt, Dr. Ian Robertson, and Dr. Matthew Allen for assistance.
Address correspondence to Dr. Marcellin-Little (denis_marcellin@ncsu.edu).

cation technologies are based on a layer-by-layer additive fabrication process in which the 3-D computer model is sliced into thin 2-D cross sections by use of a slicing algorithm. Each layer is fabricated on top of the previous layer, like the floors in a tall building, until the physical 3-D model is completed. Each FFF method forms layers with 1 specific material or more.[36] Stereolithography, developed in 1987, was the first FFF technology and is based on formation of layers of a UV-sensitive photopolymer cured by a laser beam. Fused deposition modeling is based on extrusion of a semiliquid small-diameter acrylonitrile butadiene styrene thread fused into thin layers. Three-dimensional printing is based on inkjet printing technology; a print head delivers a liquid binder onto a thin layer of plaster powder that has been spread over the build area. Once the binder has been printed, a new powder layer is spread and bonded to the previous layer. Stereolithography is reportedly more precise than 3DP for medical models.[39,40]

The purpose of the study reported here was to assess the influence of CT scan protocols (ie, radiation amount), the modeling process (thresholding), and the FFF method on the accuracy and variability of bone biomodels. We hypothesized that CT scans made by use of high-radiation settings (radiation doses higher than the mean radiation doses of all CT scans used in the study) would lead to more accurate biomodels than would CT scans made with low-radiation settings (radiation doses lower than the mean radiation doses of all CT scans used in the study), that SLA would lead to the most accurate models, and that 3DP would lead to the least accurate models.

Materials and Methods

CT scanning and modeling—A 15-year-old spayed female Basset Hound that had been euthanatized for reasons unrelated to this study was used. Informed client consent was obtained in writing. One femur was randomly selected. Three 2.5-mm-diameter holes were drilled into the lateral and medial cortices of the femoral shaft through the skin and soft tissues. The purpose of these holes was to assess the quality of the CT scans on future 3-D reconstructions. Several CT scans were performed within hours of euthanasia by use of a helical multislice CT scanner.[a] The CT scans had a scanning field of view of 210 × 210 mm, a matrix size of 512 × 512, and a pixel size of 0.41 mm (210/512 mm).

The dog was placed in dorsal recumbency with the hind limb taped in extension. Radiation detection equipment[b,c] was placed on the lateral surface of the femur. This equipment was used to detect the radiation dose received on the skin of the thigh. Two sets of 8 CT scans were collected. The scans varied in intensity and penetrability. A software function[d] aimed at decreasing the amount of radiation received by the subject was activated for some scans. The function[d] is an automatic exposure control that includes automatic tube current adaptation to the subject's size and anatomic shape combined with a tube current modulation for each tube rotation, theoretically leading to balanced image quality at low radiation dose amounts. The 16 CT scans were retroreconstructed into 158 scans with postprocessing kernels ranging from medium smooth (B30s and U30u) to sharp (B60s and U70u) to ultrasharp (B80s and U90u) and a range of windows (osteo, sinus, and abdomen). These wide ranges of kernels and windows were selected because they covered the range of windows and kernels used to image soft and hard tissues in clinical patients.[41] The 158 scans were imported in digital imaging and communications in medicine (ie, DICOM) format into a biomodeling software program,[e] and 3-D reconstructions were made. Initial thresholding was performed by lowering the threshold so that the pixels corresponding to the thin cortical bone of the femoral condyles were included, without selecting pixels outside the outer and inner surfaces of the femoral shaft. Three-dimensional renderings were created. We wanted to ensure that CT reconstructions had a high initial quality and that they did not grossly overrepresent or underrepresent the original bone. To detect the CT images that fit these criteria, a CT image rating process was designed that included the assessment of scatter (representing the initial quality of the CT), the presence of the drilled hole on the surface of the femoral shaft (confirming that the CT images did not overrepresent the original bone that had drill holes), and the presence of bone on the femoral condyles. Because bone was thinnest in that area, the presence of voids in the condyle was used to confirm that the CT images did not underrepresent the original bone. The renderings were reviewed and rated by an evaluator unaware of the CT parameters. The amount of surface irregularities (scatter) was subjectively scored as absent (0), mild (1), moderate (2), or severe (3). The appearance of the drilled holes was rated as normal (holes with sharp edges), deformed (holes visible as divots on the bone surface), or absent (holes not visible) with corresponding scores of 0, 1, or 2. The voids remaining on the femoral condyles were rated as absent, small (≤ 3 mm in diameter), or large (>

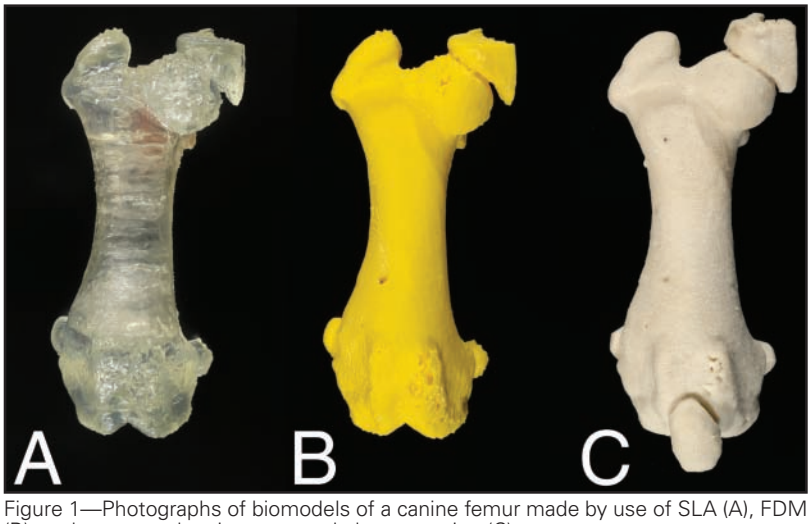

Figure 1—Photographs of biomodels of a canine femur made by use of SLA (A), FDM (B), and cyanoacrylate-impregnated plaster casting (C).

3 mm) with corresponding scores of 0, 1, or 2. The CT images were excluded from further analysis if the sum of their void score, scatter score, and drill hole score was > 2. Seventeen CT images fit these selection criteria. The mean threshold value was calculated (252 HU), and the thresholds of all 17 CT images were adjusted to that value. Threshold adjustments were recorded. The 3-D renderings were exported into FFF software, and the data were transformed from volumetric pixels (voxels) to polygon surface meshes. No smoothing of the polygon surface meshes was performed beyond the minor smoothing that occurs during the transformation from voxels to polygon surface meshes.

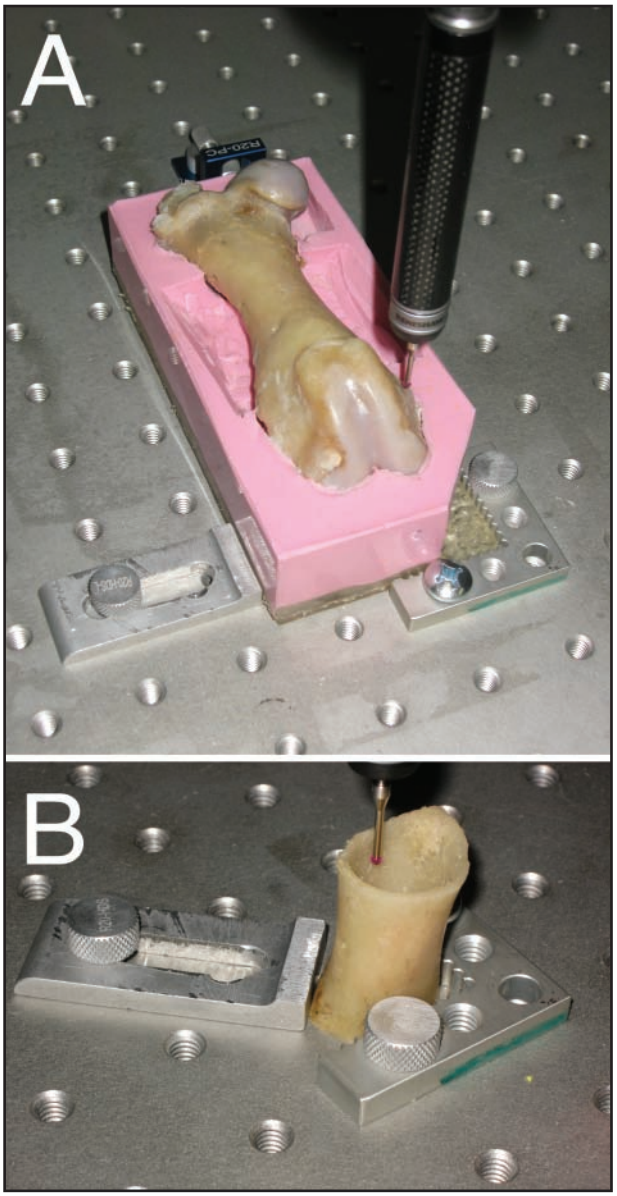

Figure 2—Photographs of a canine femur used as the source of biomodels. The femur has been placed on a custom silicone-rubber mold. Portions of the mold have been cut to allow the coordinate measurement machine to make measurements (A). The femur has been cut by use of a custom cutting jig and an oscillating saw (B). A measurement is made by use of the coordinate measurement machine. This measurement was used to calculate the cortical thickness of the caudal aspect of the distal portion of the femoral shaft.

Biomodel preparation—The cadaver was frozen until the CT images were reviewed. The cadaver was then thawed, and the femora were harvested after careful dissection. The soft tissues were removed. The femora were wrapped in saline (0.9% NaCl) solution–soaked gauze and were frozen. Three SLA, 3 FDM, and three 3DP biomodels were made on the basis of each of the 17 CT images for 153 biomodels (**Figure 1**). To accelerate SLA biomodels fabrication, SLA biomodels were built in batches of 4 biomodels in a predetermined random order. The FDM and 3DP biomodels were built one at a time in random order. The surface of the 3DP models was coated with cyanoacrylate glue to increase the strength of the models.[39]

Biomodel testing—A fixture made of room temperature (23°C) vulcanized silicone rubber was prepared on the basis of a randomly selected FDM biomodel. The fixture was cut so that the original bone and biomodels were held consistently when measured in a coordinate measurement machine.[f,g] The length, width, shaft diameter, and femoral head diameter of the original femur were measured 5 times on the coordinate measurement machine by use of a custom program (**Figure 2**). The same variables were measured once for all biomodels. The femur and biomodels were then cut across the proximal and distal aspect of the femoral shaft by use of an FDM custom jig (**Figure 3**) and an oscillating saw.[h] The cortical thickness on the cranial, lateral, caudal, and medial aspects of the proximal and distal portions of the shaft were measured 5 times for the femur and once for the biomodels by use of the coordinate measurement machine (**Figure 4**).

Statistical analysis—The coefficients of variation of the 5 sets of measurements made on the bone were calculated. The coefficients of variation of the FDM, SLA, and 3DP biomodels made in triplicate were also calculated. Homogeneity of variance across the 3 fabrication methods, FDM, SLA, and 3DP, was tested by fitting additive models to the log-transformed sample variances among the triplicate measurements, with radiation setting as a block in a randomized complete block design.[42,i] Pairwise comparisons of the variabilities of the 3 methods were made by use of the Tukey honestly significant difference test. The absolute rela-

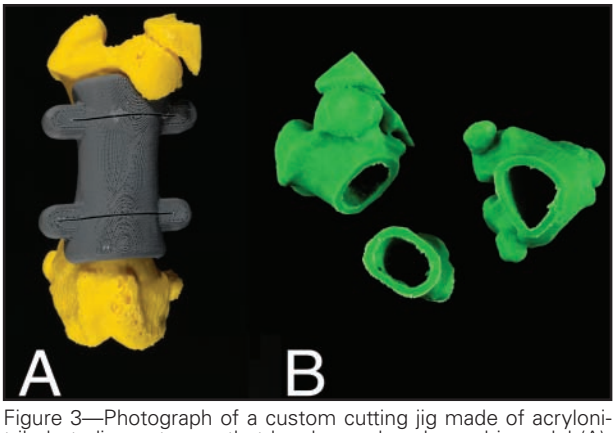

Figure 3—Photograph of a custom cutting jig made of acrylonitrile butadiene styrene that has been placed on a biomodel (A). The cutting jig has 2 thin slots guiding the blade of an oscillating saw. A biomodel has been cut in 3 parts (B).

tive errors of the FDM, SLA, and 3DP measurements from the gold standard were calculated and used as a measure of accuracy. Tests of equality of mean accuracy among the 3 fabrication methods were made by use of mixed-effects models, which used fixed effects for fabrication methods and random effects for radiation setting. The relationship between scanning parameters and biomodel accuracy was assessed by use of variable selection on separate multiple linear regression models for each outcome, with data sets of 51 observations (17 settings and 3 methods). These 51 observations were mean absolute relative deviations from the gold standard and were computed for each of 12 outcomes (diameter, length, width, femoral head size, and cortical thickness of the lateral, caudal, medial, and cranial aspects of the proximal and distal portions of the femoral shaft). A stepwise selection algorithm was used to choose scan settings that were predictive of accuracy. The effect of method on accuracy was also a candidate for entry into or removal from the accuracy model. The general form of the equations for these multiple linear regression models (before variable selection) was as follows:

$$A_i = \beta_0 + \beta_F X_{FDMi} + \beta_S X_{SLAi} + \beta_k kVp_i + \beta_x x_i + \beta_p p_i + \beta_{mr} MR_i + E_i$$

where X_{FDM} and X_{SLA} are indicator variables for the FDM and SLA methods, A_i represents the observed accuracy measurements (A_1 to A_n), β_0 is the intercept term for the model, and E_i represents the experimental errors (E_1 to E_n), assumed to be normally distributed with mean 0 and constant variance. The other predictor variables are penetrance (kVp), intensity (x), pitch (p), and measured radiation (MR) on observation i for i = 1 to 51. The criterion used for the decision about whether to add or remove a scan setting as a predictor variable was the *P* value from an F test comparing nested models. A value of $P = 0.05$ was used for all tests of significance, except for tests of partial association between accuracy and measured radiation, where a Bonferroni correction was used to control the experimentwise error rate at $P = 0.05$ for the 72 (ie, 12×6) tests involving slopes for the 3 fabrication methods and 12 image aspects (length, diameter, width, femoral head size, and the 8 cortical thickness measures).

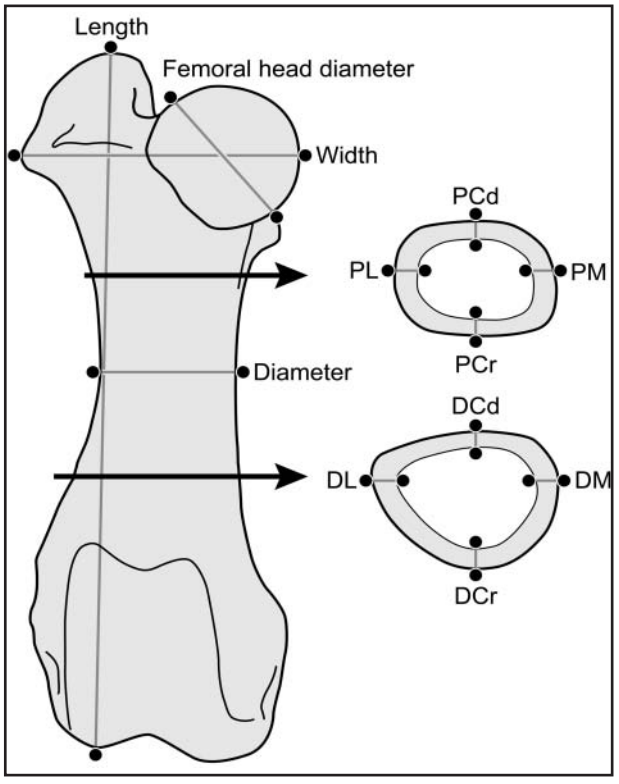

Figure 4—Illustration of a canine femur used as the source of biomodels. Variables measured on the coordinate measurement machine included femoral length, width, and diameter; femoral head diameter; the cortical thickness of the lateral (PL), caudal (PCd), medial (PM), and cranial (PCr) aspects of the proximal portion of the femoral shaft; and the cortical thickness of the lateral (DL), caudal (DCd), medial (DM), and cranial (DCr) aspects of the distal portion of the femoral shaft.

Results

The femur was 106.9 mm long and 41.7 mm wide (**Table 1**). The coefficients of variation for the 5 sets of measurements made on the bone ranged from 0.26% to 0.81% for measurements of femoral length, width, shaft diameter, and femoral head diameter and from 2.4% to 10.4% for measurements of cortical thickness (**Table 2**). The penetrability of the 17 sets of radiation configurations selected to make bone biomodels ranged from 80 to 140 kVp, and their intensity, based on x-ray tube current, ranged from 60 to 160 mAs (**Table 3**). The measured radiation for these configurations ranged from 2.28 to 19.52 mSv (mean ± SD, 7.66 ± 4.54 mSv). The threshold adjustments ranged from –138 to 84 HU (mean ± SD, 47 ± 41 HU).

Biomodel lengths, widths, shaft diameters, femoral head diameters, and cortical thicknesses were compared (Table 1). The sample variance in length measurement was significantly ($P = 0.019$) higher for FDM biomodels than for 3DP biomodels. The sample variance in diameter was significantly ($P = 0.027$) higher for FDM bio-

Table 1—Mean ± SD size (mm [accuracy {%}]) of a canine femur and 153 biomodels made by use of 3 types of FFF.

Bone and biomodel	Length	Width	Diameter	Femoral head	Cortical thickness							
					Proximal				Distal			
					Caudal	Cranial	Medial	Lateral	Caudal	Cranial	Medial	Lateral
Bone*	106.9 ± 0.27	41.7 ± 0.14	18.3 ± 0.15	22.6 ± 0.08	1.1 ± 0.05	1.4 ± 0.11	2.1 ± 0.19	1.6 ± 0.17	1.5 ± 0.05	1.8 ± 0.09	2.5 ± 0.10	1.4 ± 0.03
FDM†	105.5 ± 0.19[a] (–1.3)‡	39.6 ± 0.39[a] (–5.1)	18.2 ± 0.54 (–0.7)	19.5 ± 0.32[a] (–14)	2.2 ± 0.53[a] (103)	2.2 ± 0.54[a] (53)	3.2 ± 0.61 (49)	2.5 ± 0.59 (53)	2.2 ± 0.56[a] (51)	2.8 ± 0.62[a] (51)	3.4 ± 0.88[a,b] (34)	2.5 ± 0.60[a] (80)
SLA†	106.0 ± 0.63[a] (–0.9)	40.0 ± 0.70[b] (–4.0)	18.7 ± 0.77 (2.1)	19.4 ± 0.28[a] (–14)	2.6 ± 1.18[a] (145)	2.3 ± 0.58[a] (63)	3.5 ± 0.75 (63)	2.5 ± 0.94 (52)	2.3 ± 0.55[a] (60)	2.6 ± 0.50[a] (43)	3.0 ± 0.69[a] (19)	3.3 ± 0.79[b] (141)
3DP†	106.1 ± 0.99[b] (–0.8)	40.3 ± 0.88[b] (–3.6)	19.1 ± 0.65 (4.3)	19.1 ± 0.31[b] (–15)	2.6 ± 0.42[b] (148)	2.7 ± 0.43[b] (87)	3.2 ± 0.56 (47)	2.8 ± 0.43 (71)	2.7 ± 0.46[b] (86)	3.2 ± 0.52[b] (73)	3.5 ± 0.65[b] (38)	2.5 ± 0.43[a] (80)

*Mean value of 5 sets of measurements made by use of a coordinate measurement machine. †For FDM, SLA, and 3DP, mean value of 51 sets of measurements made by use of a coordinate measurement machine from 17 models produced in triplicate. ‡Estimated error for 51 measurements. Positive numbers indicate that biomodels were larger than the original bone.

[a,b]Within columns, means with identical superscript letters do not differ significantly ($P \geq 0.05$), indicating no significant differences in sizes among the fabrication methods.

models than for SLA biomodels. The sample variance in cortical thickness was significantly higher for FDM biomodels than for SLA biomodels for measurements made proximally and laterally ($P = 0.025$) and distally and laterally ($P = 0.018$). Differences between fabrication methods explained 2% to 29% of the total observed variation in inaccuracy, and differences among method-specific radiation configurations explained 4% to 44% of that variation (Table 2). The remainder of the variation in inaccuracy (43% to 84%, depending on the image aspect) represented differences among triplicate biomodels made from CT reconstructions with identical radiation parameters and made by use of identical fabrication methods. The biomodels were significantly inaccurate for measurement of most image aspects. They underestimated bone length, width, and femoral head diameter and overestimated cortical thickness (**Table 4**). The bone length of 3DP biomodels (99.2% accurate) was more accurate than the bone length of FDM (98.7% accurate; $P = 0.005$) and SLA biomodels (99.1% accurate; $P = 0.001$), but the femoral head size of 3DP biomodels (84.6% accurate) was less accurate than the femoral head size of FDM (85.9% accurate; $P < 0.001$) and SLA biomodels (86.3% accurate; $P < 0.001$). The bone width of FDM biomodels (94.9% accurate) was less accurate than the bone width of SLA (96.0% accurate; $P = 0.001$) and 3DP biomodels (96.5% accurate; $P = 0.009$). The cortical thickness was significantly

Table 2—Variability (%) and sources of variability among biomodels made in triplicate by use of 3 FFF methods.

					Cortical thickness							
					Proximal				Distal			
Bone and biomodels	Length	Width	Diameter	Femoral head	Caudal	Cranial	Medial	Lateral	Caudal	Cranial	Medial	Lateral
Bone*	0.26	0.34	0.81	0.33	4.6	7.8	8.7	10.4	3.7	5.0	4.1	2.4
FDM†	0.10 ± 0.07[a]	0.60 ± 0.34	0.79 ± 0.54[a]	0.93 ± 0.82	10.7 ± 8.0	6.2 ± 4.4	11.5 ± 5.7	9.5 ± 5.3[a]	8.9 ± 6.1	9.8 ± 5.8	14.4 ± 8.4	8.5 ± 5.3[a]
SLA†	0.25 ± 0.23[a,b]	0.87 ± 0.42	1.4 ± 0.5[b]	0.91 ± 0.52	14.9 ± 14.6	7.4 ± 5.5	13.0 ± 6.9	20.4 ± 21.4[b]	10.4 ± 13.1	7.9 ± 4.5	12.5 ± 10.0	13.4 ± 7.7[b]
3DP†	0.46 ± 0.64[b]	1.2 ± 1.3	1.2 ± 1.2[a,b]	0.90 ± 0.87	8.4 ± 5.8	9.9 ± 8.5	16.2 ± 10.1	9.3 ± 6.8[a,b]	11.0 ± 6.8	9.1 ± 6.5	12.7 ± 8.4	1.7 ± 8.6[a,b]
Sources of variability												
Method‡	13	15	2	24	7	14	5	4	14	16	6	29
Radiation	4	19	41	14	33	44	30	28	32	41	27	24
Other	84	65	56	62	60	43	65	68	54	43	67	47

*Coefficients of variation for 5 sets of measurements. †For FDM, SLA, and 3DP, mean ± SD of 17 coefficients of variation calculated from biomodels made in triplicate. ‡Proportion (%) of the variability from FFF method, radiation configuration, and other sources, including lack of biomodel reproducibility. Values have been rounded to whole numbers.

Table 3—Scanning and reconstruction variables of 17 CT scans used for biomodel fabrication.

Scan*	Penetrability (kVp)	x-ray tube current (mA)	Pitch	Kernel	Window	Radiation (mSv)	Scatter score†	Drilled holes score	Condylar bone score	Threshold adjustment (HU)
1	80	60	0.75	Medium smooth (B30s)	Osteo	2.71	0	1	0	–134
2	80	60	0.75	Medium smooth (B30s)	Sinus	2.71	0	1	0	–10
3	120	86	0.75	Ultrasharp (B80s)	Osteo	8.49	1	0	0	–41
4	120	86	0.75	Sharp (B60s)	Osteo	8.49	1	0	0	48
5	120	86	0.75	Ultrasharp(B80s)	Sinus	8.49	1	0	0	48
6	120	80	0.75	Ultrasharp(B80s)	Osteo	10.36	1	0	1	26
7	120	80	0.75	Ultrasharp(B80s)	Sinus	10.36	1	0	1	–5
8	120	75	0.75	Ultrasharp(B80s)	Osteo	8.40	1	0	1	66
9	120	75	0.75	Ultrasharp(B80s)	Sinus	8.40	1	0	1	12
10	120	60	0.75	Ultrasharp(B80s)	Osteo	8.14	1	0	1	12
11	120	60	0.75	Ultrasharp(B80s)	Sinus	8.14	1	0	1	48
12	120	128‡	0.75	Ultrasharp(B80s)	Sinus	12.59	1	0	1	19
13	140	128‡	0.75	Ultrasharp(B80s)	Osteo	19.52	1	0	1	84
14	80	100	0.6	Medium smooth (U30u)	Osteo	2.28	0	1	0	3
15	80	100	0.6	Medium smooth (U30u)	Sinus	2.28	0	1	0	–138
16	80	160	0.6	Medium smooth (U30u)	Osteo	3.59	0	1	0	–61
17	80	160	0.6	Medium smooth (U30u)	Sinus	3.59	0	1	0	50

*The 17 scans were selected among 158 CT retroreconstructions because of their low scatter, visible drilled holes, and complete or near complete bone on the femoral condyles. †Scatter was absent (0) or minor (1); drill holes were visible with clear edges (0) or were visible as divots in the bone surface (1); condylar bone had no holes (0) or had holes < 3 mm in diameter (1). ‡Computed tomographic scans performed with activated automatic exposure control function.

Table 4—Mean ± SD size (mm [accuracy {%}]) of 9 biomodels made from each of 17 CT reconstructions.

					Cortical thickness							
					Proximal				Distal			
Scan	Length	Width	Diameter	Femoral head	Caudal	Cranial	Medial	Lateral	Caudal	Cranial	Medial	Lateral
1	106.4 ± 1.08 (–0.4)*	40.6 ± 0.86 (–2.8)	19.4 ± 0.48 (6.1)	19.1 ± 0.12 (–15)	3.2 ± 1.3 (204)	2.7 ± 0.38 (89)	3.5 ± 0.84 (62)	3.1 ± 1.53 (91)	2.7 ± 0.28 (86)	3.3 ± 0.32 (81)	3.8 ± 0.49 (49)	3.3 ± 0.54 (139)
2	106.3 ± 0.91 (–0.6)	40.3 ± 0.49 (–3.4)	19.3 ± 0.45 (5.1)	19.1 ± 0.24 (–15)	2.9 ± 0.45 (174)	3.0 ± 0.32 (112)	4.1 ± 0.58 (91)	3.4 ± 0.35 (106)	2.8 ± 0.44 (94)	3.5 ± 0.35 (90)	3.8 ± 0.43 (49)	3.3 ± 0.61 (139)
3	106.0 ± 0.26 (–0.8)	40.0 ± 0.33 (–4.1)	18.4 ± 0.32 (0.3)	19.2 ± 0.23 (–15)	2.0 ± 0.31 (93)	2.2 ± 0.43 (56)	3.0 ± 0.68 (41)	2.4 ± 0.34 (45)	2.0 ± 0.40 (40)	2.5 ± 0.44 (38)	2.8 ± 0.54 (12)	2.3 ± 0.32 (67)
4	105.5 ± 0.50 (–1.3)	39.9 ± 0.32 (–4.5)	18.3 ± 0.43 (–0.2)	19.3 ± 0.20 (–15)	2.2 ± 0.28 (106)	2.2 ± 0.28 (53)	3.0 ± 0.46 (42)	2.3 ± 0.23 (42)	2.1 ± 0.34 (47)	2.6 ± 0.26 (42)	3.0 ± 0.56 (20)	2.5 ± 0.51 (86)
5	105.7 ± 0.36 (–1.1)	40.1 ± 0.34 (–4.0)	18.2 ± 0.43 (–0.6)	19.3 ± 0.19 (–15)	2.0 ± 0.35 (86)	2.2 ± 0.41 (54)	3.3 ± 0.48 (54)	2.1 ± 0.44 (27)	2.2 ± 0.35 (50)	2.6 ± 0.40 (39)	3.0 ± 0.55 (20)	2.4 ± 0.38 (73)
6	105.3 ± 1.23 (–1.5)	40.1 ± 0.79 (–3.9)	18.3 ± 0.56 (0.1)	19.5 ± 0.33 (–14)	2.1 ± 0.45 (101)	2.1 ± 0.39 (50)	3.2 ± 0.40 (48)	2.2 ± 0.40 (36)	2.1 ± 0.40 (43)	2.6 ± 0.37 (42)	3.0 ± 0.40 (21)	2.2 ± 0.27 (64)
7	105.8 ± 0.44 (–1.0)	39.5 ± 0.51 (–5.3)	18.1 ± 0.53 (–1.0)	19.5 ± 0.42 (–14)	2.1 ± 0.41 (102)	2.0 ± 0.35 (41)	3.0 ± 0.45 (41)	2.2 ± 0.36 (36)	2.3 ± 0.88 (58)	2.5 ± 0.42 (38)	2.6 ± 0.73 (3.1)	2.6 ± 0.79 (88)
8	105.2 ± 1.18 (–1.6)	39.1 ± 1.14 (–6.4)	18.2 ± 0.58 (–0.8)	19.6 ± 0.29 (–13)	2.0 ± 0.37 (85)	2.1 ± 0.32 (48)	3.1 ± 0.32 (44)	2.3 ± 0.46 (38)	2.1 ± 0.33 (46)	2.6 ± 0.39 (44)	3.0 ± 0.49 (19)	2.3 ± 0.42 (70)
9	105.9 ± 0.37 (–0.9)	39.7 ± 0.23 (–4.8)	18.1 ± 0.36 (–1.2)	19.5 ± 0.18 (–14)	2.1 ± 0.37 (95)	2.0 ± 0.60 (42)	2.8 ± 0.29 (32)	2.1 ± 0.27 (26)	2.1 ± 0.35 (45)	2.5 ± 0.53 (35)	2.7 ± 0.44 (7.6)	2.4 ± 0.50 (75)
10	106.0 ± 0.49 (–0.8)	39.5 ± 0.42 (–5.3)	18.1 ± 0.41 (–1.1)	19.6 ± 0.50 (–13)	2.1 ± 0.41 (98)	1.9 ± 0.34 (34)	2.9 ± 0.42 (36)	2.4 ± 0.31 (46)	2.0 ± 0.30 (38)	2.5 ± 0.53 (35)	2.8 ± 0.34 (11)	2.5 ± 0.80 (82)
11	106.1 ± 0.31 (–0.8)	39.6 ± 0.28 (–5.1)	18.2 ± 0.37 (–0.6)	19.4 ± 0.28 (–14)	2.1 ± 0.28 (99)	2.0 ± 0.34 (41)	2.9 ± 0.27 (34)	2.2 ± 0.33 (37)	2.2 ± 0.36 (54)	2.5 ± 0.22 (37)	3.2 ± 0.52 (25)	2.4 ± 0.36 (78)
12	106.0 ± 0.36 (–0.9)	39.5 ± 0.51 (–5.4)	18.2 ± 0.39 (–0.9)	19.6 ± 0.45 (–13)	2.0 ± 0.32 (93)	2.1 ± 0.34 (47)	2.9 ± 0.30 (35)	2.3 ± 0.51 (43)	2.1 ± 0.44 (48)	2.5 ± 0.53 (36)	2.8 ± 0.43 (13)	2.4 ± 0.34 (77)
13	106.0 ± 0.94 (–0.9)	39.8 ± 1.16 (–4.6)	18.3 ± 0.87 (–0.2)	19.5 ± 0.46 (–14)	2.0 ± 0.23 (86)	1.9 ± 0.23 (34)	3.0 ± 0.60 (37)	2.5 ± 0.74 (51)	2.0 ± 0.37 (41)	2.4 ± 0.29 (29)	3.2 ± 0.83 (26)	2.5 ± 0.72 (82)
14	105.7 ± 0.72 (–1.2)	40.4 ± 0.76 (–3.2)	19.5 ± 0.59 (6.7)	19.1 ± 0.21 (–16)	3.1 ± 0.42 (197)	3.1 ± 0.31 (120)	3.9 ± 0.43 (81)	3.1 ± 0.65 (89)	3.0 ± 0.20 (105)	3.4 ± 0.58 (87)	4.0 ± 0.75 (60)	3.3 ± 0.63 (141)
15	105.9 ± 0.49 (–1.0)	40.4 ± 0.53 (–3.2)	19.5 ± 0.45 (6.7)	19.1 ± 0.29 (–15)	2.8 ± 0.39 (168)	3.0 ± 0.19 (109)	3.6 ± 0.91 (68)	2.9 ± 0.36 (80)	2.8 ± 0.34 (96)	3.4 ± 0.49 (86)	4.0 ± 1.14 (57)	3.4 ± 1.08 (148)
16	106.0 ± 0.42 (–0.9)	40.4 ± 0.47 (–3.1)	19.6 ± 0.39 (7.1)	19.1 ± 0.28 (–15)	3.5 ± 0.99 (229)	3.0 ± 0.41 (110)	3.6 ± 0.57 (69)	3.4 ± 0.37 (110)	3.3 ± 0.57 (127)	3.6 ± 0.46 (96)	4.4 ± 0.45 (73)	3.5 ± 0.79 (153)
17	106.0 ± 0.46 (–0.9)	40.6 ± 0.65 (–2.7)	19.7 ± 0.50 (7.4)	19.1 ± 0.23 (–15)	3.5 ± 1.43 (229)	3.0 ± 0.14 (113)	4.0 ± 0.63 (88)	3.2 ± 0.33 (94)	2.9 ± 0.42 (98)	3.5 ± 0.32 (93)	3.8 ± 0.49 (49)	3.4 ± 0.72 (148)

*Estimated error for measurements from 9 biomodels.

Table 5—Influence of CT variables on the accuracy of 153 biomodels made by use of 3 types of FFF.

Variables	Length	Width	Diameter	Femoral head	Cortical thickness							
					Proximal				Distal			
					Caudal	Cranial	Medial	Lateral	Caudal	Cranial	Medial	Lateral
Penetrability (kVp)	–	+ (< 0.001)	+ (< 0.001)	+ (< 0.001)	+ (< 0.001) + (0.022)	+ (< 0.001) + (0.030)	+ (< 0.001)	+ (< 0.001)	+ (< 0.001) + (0.004)	+ (< 0.001) + (0.020)	+ (< 0.001)	+ (< 0.001)
Intensity (mA)	–	–	–	–	–	–	–	–	–	–	–	–
Pitch	–	–	–	–	–	–	–	–	–	–	+ (0.049)	–
Radiation dose (mSv)	–	–	+ (0.025)	–	–	–	–	+ (< 0.001)	–	–	+ (0.028)	+ (0.022)
Slope*	0.0001	0.0015	–0.003	–0.001	–0.082	–0.052	–0.028	–0.041	–0.045	–0.042	–0.027	–0.052
Correlation coefficient (r^2)	0.206	0.561	0.607	0.633	0.725	0.858	0.619	0.733	0.824	0.902	0.700	0.804
Threshold adjustment												
Correlation coefficient (r^2)	0.145	0.014	0.129	0.083	0.012	–0.023	–0.021	0.049	–0.003	–0.034	0.043	0.110
P value	0.300	0.922	0.356	0.555	0.932	0.868	0.884	0.726	0.983	0.809	0.759	0.435

A plus sign indicates that the variable influenced biomodel accuracy (and associated *P* values); a minus sign indicates that the variable did not influence biomodel accuracy. *Positive slopes indicate that biomodels become less accurate with increasing radiation doses; negative slopes indicate that biomodels become more accurate with increasing radiation doses. A –0.041 slope (eg, in the measurement of the accuracy of cortical thickness proximally and laterally) indicates that cortical thickness becomes 4.1% more accurate with each increase of 1 mSv of radiation dose.

($P < 0.001$) more accurate for FDM biomodels than for 3DP biomodels in 4 of 8 regions: distal caudal (66.0% vs 53.8% accurate), distal cranial (66.7% vs 57.7%), proximal caudal (49.0% vs 40.3%), and proximal cranial (65.5% vs 53.4%).

There was no evidence of any linear association between threshold adjustments and biomodel accuracy (**Table 5**). The accuracy of FDM biomodels increased significantly ($P < 0.001$) with higher measured radiation for femoral head diameter and for all 8 cortical thickness measurements. The accuracy of SLA biomodels increased significantly ($P < 0.001$) with higher measured radiation for bone width and for 7 of 8 cortical thickness measurements. The accuracy of 3DP biomodels increased significantly ($P < 0.001$) with higher measured radiation for femoral shaft diameter and for 4 of 8 cortical thickness measurements. The accuracy of biomodels increased with an increased x-ray beam penetrability and, to a lesser extent, with an increase in x-ray tube current (intensity) or an increase in measured radiation. Increases in radiation doses led to a small increase in the accuracy of biomodel diameter and a moderate increase in the accuracy of biomodel cortical thickness.

Discussion

The purpose of the study reported here was to assess the effect of radiation amounts and FFF methods on the accuracy of biomodels. For that purpose, the femur of a chondrodystrophic dog (Basset Hound) was selected specifically because the bone would have large features that would enhance the ability to assess the accuracy of biomodels and would be short, increasing fabrication speed and decreasing the fabrication cost of the biomodels. The femur was selected among all long bones because of its prominent anatomic features, because it is the site of many orthopedic procedures, and because it is routinely used in biomodeling projects. No evidence of orthopedic disease was found in the hind limb. Because the dog was old, the femur may have had a low bone mineral content. Bone mineral content is reported as decreased in dogs > 10 years of age, compared with dogs < 10 years of age, in 1 report.[43] The influence of bone mineral density on biomodel accuracy is not known and was beyond the scope of the present study.

The study was based on CT because it is the most accurate method to image bone tissue. Computed tomography had superior accuracy to magnetic resonance imaging (0.9% and –3.5%, respectively) when imaging bone in 1 study.[44] Helical multislice CT scanning was used in that study.[44] Helical multislice scanning is reportedly more accurate than transverse single-slice scanning because it images thin, overlapping slices without an increase in scanning time or radiation dose.[45] Three-dimensional reconstructions were optimized by a slice overlap of 25% to 75% in that report,[45] and a pitch increase from 1.0 to 1.5 did not negatively affect the quality of 3-D reconstructions at a slice thickness of 2 mm. In that study, higher pitches were found to decrease scanning time and radiation dose: a pitch of 1.5 resulted in a 34% reduction in radiation dose to the patient, compared with a pitch of 1.0. Helical scanning, however, leads to an increased volume of the subject being irradiated (overbeaming), compared with transverse scanning. Overbeaming is attributable in part to the fact that helical scanning requires an additional rotation at the beginning and end of each acquisition. A helical CT with a pitch > 1 combined with overlapping reconstructions provides improved 3-D imaging with greater volume acquisition but overall less radiation to the patient.[45] In the present study, the femur was scanned multiple times by use of a wide range of CT capture and postprocessing variables. The 17 most accurate retroreconstructions were identified and used to build 9 biomodels of each of these retroreconstructions by use of 3 FFF methods (3 models/method × 3 methods). The retroreconstructions that led to the most realistic renderings had a wide variety of CT variables and were associated with radiation exposure ranging from approximately 2 to 20 mSv. Only 2 of the 17 best retroreconstructions were reconstructed from CT scans that had been made with the automatic exposure control function[d] activated. These CT scans were associated with high x-ray tube current and the highest radiation exposures. Because we did not directly compare the accuracy of retroreconstructions made with and without the automatic exposure control function,[d] its effect on biomodel accuracy could not be assessed in this study. High radiation settings increased the accuracy for 22 of the 36 variables measured in the study: 9 of 12 variables for SLA biomodels, 8 of 12 variables for FDM biomodels, and 5 of 12 variables for 3DP biomodels. The accuracy of the remaining 14 variables was not increased by the use of high radiation settings. An increase in x-ray beam penetrability (kVp) led to an increase in biomodel accuracy for all variables measured except biomodel length. An increase in x-ray tube current (mA) had a positive effect on the accuracy of a few variables (4/12) and had no effect on most variables. A decrease in pitch had a positive effect on the accuracy of 1 variable. The

hypothesis that CT scans made by use of high radiation settings would lead to more accurate biomodels than CT scans made with low radiation settings was therefore accepted. Low radiation settings had more influence on the lack of cortical thickness accuracy than on the lack of accuracy of the outside dimensions of the bone. The findings of this study indicate that low-radiation CT scanning represents a minor compromise with regard to biomodel accuracy. Although radiation amounts seemingly do not represent a clear concern for companion animals, they are a public health concern for humans, particularly for children. Children in the United States undergo 4 to 6 million CT scans/y. The number of CT scans has increased 7-fold since 1981, and CT scans are contributing to 40% of the population's collective radiation dose.[46] Pediatric CT scanning protocols have been developed to reduce radiation exposure as much as possible. In a study[47] in humans, the radiation doses received during CT scanning were 4.85 ± 1.74 mSv for pelvic studies, 3.09 ± 1.37 mSv for hip studies, and 0.07 ± 0.05 mSv for ankle studies. These doses were similar to that of the low radiation setting used in the present study.

Thresholding is a somewhat subjective modeling step that affects the amount of pixels selected when a 3-D rendering is built from the CT scan.[35] Lowering the threshold increases cortical thickness, and increasing the threshold leads to the presence of voids in bone regions with the thinnest cortices. The effect of thresholding was controlled by use of an identical threshold for the 17 CT radiation profiles used in the study. Initial thresholding was performed, the mean value of all initially selected thresholds was calculated, and the thresholds of all CT images were adjusted to that mean value. Statistical analyses confirmed that threshold adjustments had no effect on biomodel accuracy.

Overall variability among models was low. A significant portion of that variability was the result of differences among biomodels built by use of the same fabrication method and from identical CT variables. This variability was most likely caused by the imperfect repeatability of biomodel fabrication, processing, and measurement methods. The 3 FFF methods were selected because they covered the full range of FFF techniques: use of an energy beam to cure a liquid photopolymer (SLA), use of 3DP, and use of an extrusion process (FDM). Although statistical differences in accuracy and reproducibility between the 3 FFF methods were present, no clear practical differences among methods were identified. The hypotheses that SLA biomodels were most accurate and 3DP biomodels were least accurate were therefore rejected. The portion of the biomodel variability resulting from differences among FFF methods was small (2% to 29%, depending on the variables). The 3 methods accurately reproduced the external dimensions of the femoral shaft (length, width, and diameter). The size of the femoral head was underestimated by approximately 15% (3 mm) by all 3 methods. This was mainly attributable to the fact that the femur had articular cartilage on the femoral head, but the biomodels did not. The articular cartilage thickness of the femoral head of dogs has been reported to be 0.67 ± 0.01 mm.[48] Also, the thin subchondral bone in that region may not have been accurately imaged during the thresholding process. All methods, particularly the 3DP, grossly overestimated the cortical thickness of the femoral shaft. Because all FFF methods overestimated the cortical thickness, it is possible that some of the lack of accuracy was the result of the scanning and modeling process. Scanning variables, including slice thickness and gantry orientation, and smoothing during modeling are sources of inaccuracy in biomodel fabrication.[19,35] Because they had accurate outside dimensions, the biomodels made in the present study would be suited to the assessment of bone shape and to rehearsing surgical procedures involving the placement of external implants (ie, bone plates and external skeletal fixation frames). The lack of cortical thickness accuracy, however, makes these models less suitable to rehearsing or planning surgical procedures involving the precise placement of implants inside the endosteal cavity (ie, a pressfit femoral stem).

Freeform fabrication method availability, practicality, cost, and biomodel durability should be taken into consideration before selecting a specific fabrication method. In the present study, 3DP models had the lowest cost and SLA models had the highest cost. Stereolithography models are considered to be the gold standard for rapid medical prototyping applications and are cited as a more efficient process for larger parts but more labor-intense at higher costs.[49] Model accuracy and reproducibility could possibly be improved by the use of improved FFF methods. The accuracy of SLA, for example, may be improved by the use of a blade sweeping across the build platform between each layer.[50]

a. Siemens SOMATOM Sensation 16-slice configuration, Siemens Medical Solutions, Malvern, Pa.
b. 35050AT Triad TnT Dosimeter, Fluke, Everett, Wash.
c. 96035B 15-cc ion chamber, Fluke, Everett, Wash.
d. CARE dose 4D, Siemens Medical Solutions, Malvern, Pa.
e. Mimics 10.11, Materialise, Ann Arbor, Mich.
f. Discovery II D-8, Sheffield, Fond du Lac, Wis.
g. MH20i touch probe, Renishaw, Hoffman Estates, Ill.
h. Stryker II, Stryker Instruments Inc, Kalamazoo, Mich.
i. SAS, version 9.1.3, SAS Institute Inc, Cary, NC.

References

1. Chassagne JF, Corbel S, Gimenez F, et al. Rapid prototyping and bone reconstruction. *Ann Chir Plas Esthet* 1999;44:515–524.
2. Barker TM, Earwaker WJ, Lisle DA. Accuracy of stereolithographic models of human anatomy. *Australas Radiol* 1994;38:106–111.
3. Chow J, Hui E, Lee PK, et al. Zygomatic implants—protocol for immediate occlusal loading: a preliminary report. *J Oral Maxillofac Surg* 2006;64:804–811.
4. Dai KR, Yan MN, Zhu ZA, et al. Computer-aided custom-made hemipelvic prosthesis used in extensive pelvic lesions. *J Arthrop* 2007;22:981–986.
5. D'Urso PS, Barker TM, Earwaker WJ, et al. Stereolithographic biomodelling in cranio-maxillofacial surgery: a prospective trial. *J Craniomaxillofac Surg* 1999;27:30–37.
6. D'Urso PS, Williamson OD, Thompson RG. Biomodeling as an aid to spinal instrumentation. *Spine* 2005;30:2841–2845.
7. El-Ghannam A, Cunningham L Jr, Pienkowski D, et al. Bone engineering of the rabbit ulna. *J Oral Maxillofac Surg* 2007;65:1495–1502.
8. Harrysson OLA, Cormier DR, Marcellin-Little DM, et al. Rapid prototyping for treatment of canine limb deformities. *Rapid Prototyping J* 2003;9:37–42.

9. Hildreth BE, Marcellin-Little DJ, Roe SC, et al. In vitro evaluation of five canine tibial plateau leveling methods. *Am J Vet Res* 2006;67:693–700.
10. Hurson C, Tansey A, O'Donnchadha B, et al. Rapid prototyping in the assessment, classification and preoperative planning of acetabular fractures. *Injury* 2007;38:1158–1162.
11. Hu YJ, Hardianto A, Li SY, et al. Reconstruction of a palatomaxillary defect with vascularized iliac bone combined with a superficial inferior epigastric artery flap and zygomatic implants as anchorage. *Int J Oral Maxillofac Surg* 2007;36:854–857.
12. Kacl GM, Zanetti M, Amgwerd M, et al. Rapid prototyping (stereolithography) in the management of intra-articular calcaneal fractures. *Eur Radiol* 1997;7:187–191.
13. Lo LJ, Chen YR, Tseng CS, et al. Computer-aided reconstruction of traumatic fronto-orbital osseous defects: aesthetic considerations. *Chang Gung Med J* 2004;27:283–291.
14. Owen BD, Christensen GE, Reinhardt JM, et al. Rapid prototype patient-specific drill template for cervical pedicle screw placement. *Comput Aided Surg* 2007;12:303–308.
15. Paiva WS, Amorim R, Bezerra DA, et al. Application of the stereolithography technique in complex spine surgery. *Arq Neuropsiquiatr* 2007;65:443–445.
16. Mizutani J, Matsubara T, Fukuoka M, et al. Application of full-scale three-dimensional models in patients with rheumatoid cervical spine. *Eur Spine J* 2008;17:644–649.
17. Robiony M, Salvo I, Costa F, et al. Virtual reality surgical planning for maxillofacial distraction osteogenesis: the role of reverse engineering rapid prototyping and cooperative work. *J Oral Maxillofac Surg* 2007;65:1198–1208.
18. Sinn DP, Cillo JE Jr, Miles BA. Stereolithography for craniofacial surgery. *J Craniofac Surg* 2006;17:869–875.
19. Winder J, Bibb R. Medical rapid prototyping technologies: state of the art and current limitations for application in oral and maxillofacial surgery. *J Oral Maxillofac Surg* 2005;63:1006–1015.
20. Armillotta A, Bonhoeffer P, Dubini G, et al. Use of rapid prototyping models in the planning of percutaneous pulmonary valved stent implantation. *Proc Inst Mech Eng H* 2007;221:407–416.
21. Berry E, Marsden A, Dalgarno KW, et al. Flexible tubular replicas of abdominal aortic aneurysms. *Proc Inst Mech Eng H* 2002;216:211–214.
22. Chetty A, Steynberg T, Moolman S, et al. Hydroxyapatite-coated polyurethane for auricular cartilage replacement: an in vitro study. *J Biomed Mater Res A* 2008;84:475–482.
23. Cooke MN, Fisher JP, Dean D, et al. Use of stereolithography to manufacture critical-sized 3D biodegradable scaffolds for bone ingrowth. *J Biomed Mater Res B Appl Biomater* 2003;64:65–69.
24. Harrysson OL, Hosni YA, Nayfeh JF. Custom-designed orthopedic implants evaluated using finite element analysis of patient-specific computed tomography data: femoral-component case study. *BMC Musculoskelet Disord* 2007;8:91.
25. Henry JA, O'Sullivan G, Pandit AS. Using computed tomography scans to develop an ex-vivo gastric model. *World J Gastroenterol* 2007;13:1372–1377.
26. Hiramatsu H, Tokashiki R, Yamaguchi H, et al. Three-dimensional laryngeal model for planning of laryngeal framework surgery. *Acta Otolaryngol* 2006;126:515–520.
27. Jacobs S, Grunert R, Mohr FW, et al. 3D-imaging of cardiac structures using 3D heart models for planning in heart surgery: a preliminary study. *Interact Cardiovasc Thorac Surg* 2008;7:6–9.
28. Ngan EM, Rebeyka IM, Ross DB, et al. The rapid prototyping of anatomic models in pulmonary atresia. *J Thorac Cardiovasc Surg* 2006;132:264–269.
29. Peltola SM, Melchels FP, Grijpma DW, et al. A review of rapid prototyping techniques for tissue engineering purposes. *Ann Med* 2008;40:268–280.
30. Schievano S, Migliavacca F, Coats L, et al. Percutaneous pulmonary valve implantation based on rapid prototyping of right ventricular outflow tract and pulmonary trunk from MR data. *Radiology* 2007;242:490–497.
31. Sodian R, Weber S, Markert M, et al. Stereolithographic models for surgical planning in congenital heart surgery. *Ann Thorac Surg* 2007;83:1854–1857.
32. Wang X, Yan Y, Zhang R. Rapid prototyping as a tool for manufacturing bioartificial livers. *Trends Biotechnol* 2007;25:505–513.
33. Watts DM, Sutcliffe CJ, Morgan RH, et al. Anatomical flow phantoms of the nonplanar carotid bifurcation, part I: computer-aided design and fabrication. *Ultrasound Med Biol* 2007;33:296–302.
34. Knox K, Kerber CW, Singel SA, et al. Stereolithographic vascular replicas from CT scans: choosing treatment strategies, teaching, and research from live patient scan data. *AJNR Am J Neuroradiol* 2005;26:1428–1431.
35. Choi JY, Choi JH, Kim NK, et al. Analysis of errors in medical rapid prototyping models. *Int J Oral Maxillofac Surg* 2002;31:23–32.
36. Chua CK, Leong KF, Lim CS. *Rapid prototyping: principles and applications*. Singapore: World Scientific, 2003.
37. Keating AP, Knox J, Bibb R, et al. A comparison of plaster, digital and reconstructed study model accuracy. *J Orthod* 2008;35:191–201.
38. Klein HM, Schneider W, Alzen G, et al. Pediatric craniofacial surgery: comparison of milling and stereolithography for 3D model manufacturing. *Pediatr Radiol* 1992;22:458–460.
39. Silva DN, Gerhardt de Oliveira M, Meurer E, et al. Dimensional error in selective laser sintering and 3D-printing of models for craniomaxillary anatomy reconstruction. *J Craniomaxillofac Surg* 2008;36:443–449.
40. Ibrahim D, Broilo TL, Heitz C, et al. Dimensional error of selective laser sintering, three-dimensional printing and PolyJet models in the reproduction of mandibular anatomy. *J Craniomaxillofac Surg* 2009;37:167–173.
41. Bredenhöller C, Feuerlein U. *SOMATOM Sensation 10/16 application guide*. 2nd ed. Munich: Siemens AG, 2005;580.
42. Steel RGD, Torrie JH, Dickey DA. *Principles and procedures of statistics: a biometrical approach*. 3rd ed. New York: McGraw-Hill, 1996.
43. Lorinson K, Loebcke S, Skalicky M, et al. Signalment differences in bone mineral content and bone mineral density in canine appendicular bones. A cadaveric study. *Vet Comp Orthop Traumatol* 2008;21:147–151.
44. White D, Chelule KL, Seedhom BB. Accuracy of MRI vs CT imaging with particular reference to patient specific templates for total knee replacement surgery. *Int J Med Robot* 2008;4:224–231.
45. Hopper KD, Pierantozzi D, Potok PS, et al. The quality of 3D reconstructions from 1.0 and 1.5 pitch helical and conventional CT. *J Comput Assist Tomogr* 1996;20:841–847.
46. Brenner D, Elliston C, Hall E, et al. Estimated risks of radiation-induced fatal cancer from pediatric CT. *AJR Am J Roentgenol* 2001;176:289–296.
47. Biswas D, Bible JE, Bohan M, et al. Radiation exposure from musculoskeletal computerized tomographic scans. *J Bone Joint Surg Am* 2009;91:1882–1889.
48. Daubs BM, Markel MD, Manley PA. Histomorphometric analysis of articular cartilage, zone of calcified cartilage, and subchondral bone plate in femoral heads from clinically normal dogs and dogs with moderate or severe osteoarthritis. *Am J Vet Res* 2006;67:1719–1724.
49. Cohen A, Laviv A, Berman P, et al. Mandibular reconstruction using stereolithographic 3-dimensional printing modeling technology. *Oral Surg Oral Med Oral Pathol Oral Radiol Endod* 2009;108:661–666.
50. Jacobs PF, Reid DT. Software architecture. In: Jacobs PF, ed. *Rapid prototyping & manufacturing: fundamentals of stereolithography*. Dearborn, Mich: Society of Manufacturing Engineers, 1992;121.